Modeling and mechanism of the adsorption of copper ion onto natural bamboo sawdust

Xue-Tao Zhao [a,b], Teng Zeng [a], Xue-Yan Li [b], Zhang Jun Hu [a], Hong-Wen Gao [a,*], Zhi Xie [c]

[a] State Key Laboratory of Pollution Control and Resource Reuse, College of Environmental Science and Engineering, Tongji University, Shanghai 200092, People's Republic of China
[b] School of Environmental Science and Engineering, Suzhou University of Science and Technology, People's Republic of China
[c] National Synchrotron Radiation Laboratory, University of Science and Technology of China, Hefei, Anhui 230029, People's Republic of China

ARTICLE INFO

ABSTRACT

The sorption of copper ions onto natural bamboo sawdust with cellulose–lignin polymeric structure strongly depends on pH. The adsorption capacity for copper ions increases as increasing pH and copper loadings. The fitting of copper pH boundary curve by NEM surface complexation models shows that: three-sites model including the ion exchange reaction of permanent charge fits better than two-sites model. The incorporation of the hydrated ion reaction gives better fitting results. XAFS study shows that: copper ions mainly form inner complexation with sawdust, but there is no obvious evidence on the complexation of carboxylic acid groups with copper ions. EXAFS fitting result shows that: as pH rises, the spatial configuration of copper ions shifts from tetrahedron to octahedron. Meanwhile the increase in the coordination number indicates that hydrated copper ions participate in the adsorption. Both XANES and EXFAS spectrum offer a similar explanation for copper adsorption in the range of experimental and fitting errors.

1. Introduction

Adsorption technology was a kind of effective water and wastewater treatment technology. The most widely used adsorbent was activated carbon in industry. However, it was an expensive material although it had regenerative capacity. Therefore, in recent years, abundant research was conducted to find cheaper adsorbent to remove heavy metals in drinking water and wastewater. Sawdust as a low-cost adsorbent which is carbohydrate natural polymer can be used to remove heavy metals from water (Ahmed, 2011; Lee, 2001; Naiya, Bhattacharya, & Das, 2008; Shukla, Zhang, Dubey, Margrave, & Shukla, 2002; Yasemin & Zek, 2007; Yu, Shukla, & Dorris, 2003). Sawdust itself was a kind of solid waste, which needed to be reused. In the paper, the authors applied natural bamboo sawdust to adsorb copper ion in the solution.

The main components of natural bamboo sawdust are cellulose, hemicellulose and lignin. Among them, cellulose and hemicellulose, which account for about 50% of the dry matter, belong to the category of carbohydrates. Most recent studies on the adsorption of heavy metals onto sawdust applied empirical models like Langmuir and Freundlich models to evaluate the binding property. The parameters of these models had no specific physical meanings and did not offer a mechanistic explanation for adsorption (Ahmed, 2011; Lee, 2001; Naiya et al., 2008; Shukla et al., 2002; Yasemin & Zek, 2007; Yu et al., 2003). In the paper, the authors attempted to apply surface complexation model to explain a specific mechanism of the adsorption of copper ion onto natural bamboo sawdust. The model had made great success at describing the sorption reaction of natural polysaccharide (Guo, Zhang, & Shan, 2008; Reddad, Cerente, Andres, & Clolrec, 2002), and wheat bran (Ravat, Dumonceau, & Monteil-Rivera, 2000).

The sorption onto sawdust strongly depends on their charging status. In part 1 of this series (Zhao, Zeng, Hu, Gao, & Zou, 2012), the non-electrostatic surface complexation model (NEM) (Kohler, Curtis, David, Meece, & Davis, 2004; Marmier & Fromage, 1999) was used to account for the proton binding behavior of bamboo sawdust. The intrinsic acidity constants and the density of different surface functional groups were obtained (Table 2 of Zhao et al., 2012). For these sites, the binding of proton and metal ions are closely related. The fitting data with alkali side pH 3.5 as starting point were chosen for copper ions adsorption fitting in the paper (Table 2 of Zhao et al., 2012). Using the proton binding constants and site density, metal ion adsorption curves can be projected and parameters such as metal ion binding constants and coordination numbers can be predicted by the software FITEQL 4.0 (Herbelin & Westall, 1999).

To investigate the adsorption mechanisms of heavy metals at the molecular level, a spectroscopic approach was preferred, such as IR (Xu, Axe, Yee, & Dyer, 2006), XRD (Steinike, Lutz, Wark, & Jancke, 1994), EPR (Xia, Bleam, & Helmke, 1997; Xia, Mehadi, Taylor,

---

Table 1
Acid–base titration surface complexation reaction.

Species	Mass action relation	Equilibrium constant	
>SO$^-$	>SOH $\Leftrightarrow$ > SO$^-$ + H$^+$	$K_{SO^-} = \dfrac{[> SO^-]\{H^+\}}{[> SOH]}$	(1)
>SOCu$^+$	>SOH + Cu^{2+} = > SOCu$^+$ + H$^+$	$K_{SOCu^+} = \dfrac{[> SOCu^+]\{H^+\}}{[> SOH]\{Cu^{2+}\}}$	(2)
(> SO)$_2$Cu	2 > SOH + Cu^{2+} = (> SO)$_2$Cu + 2H$^+$	$K_{(SO)_2Cu} = \dfrac{[> (SO)_2Cu]\{H^+\}^2}{[> SOH]^2\{Cu^{2+}\}}$	(3)
>SOCuOH	>SOH + Cu^{2+} + H$_2$O = > SOCuOH + 2H$^+$	$K_{SOCuOH} = \dfrac{[> SOCuOH]\{H^+\}^2}{[> SOH]\{Cu^{2+}\}}$	(4)
>Z$_2$Cu	2 > ZK + Cu^{2+} $\rightarrow$ > Z$_2$Cu + 2K$^+$	$K_{Z_2Cu} = \dfrac{[> Z_2Cu]\{K^+\}^2}{[> ZK]^2\{Cu^{2+}\}}$	(5)

Where ">SOH" represents both high proton affinity sites and low proton affinity sites, ">ZK" represents permanently charged sites, "{}" represents activity and "[]" represents concentration.

& Bleam, 1997), and XAFS. As for the infrared spectrum, the spectrum change of absorbent was often less obvious, so it was difficult to tease out the binding mechanism of heavy metals in this study. XRD mainly targeted at the adsorption of crystal particles. Although the g-value of EPR spectrum was sensitive to the type of ligands coordinating the metal atom, it was impossible to estimate the bond distances or bond angles from g-value shifts, which only applied to a few paramagnetic metals (Xia, Bleam, et al., 1997; Xia, Mehadi, et al., 1997). The development of the synchrotron radiation-based X-ray absorption near edge structure (XANES) and extended X-ray absorption fine structure (EXAFS) technique during this past decade had proven to be a powerful tool in environmental research as it probed the local structure of atoms (or ions) and electronic structure of complexation mechanisms (Alcacio, Hesterberg, & Chou, 2001; Blair & Goddard, 1980; Dupont, Guillon, & Bouanda, 2002; Garcia et al., 1989; Joyner, 1980; Kau, Spira-Solomon, Penner-Hahn, Hodgson, & Solomon, 1987; Scheidegger, Lamble, & Sparks, 1996; Xia, Bleam, et al., 1997; Xia, Mehadi, et al., 1997).

Due to the rarity of synchrotron radiation source, few XAFS studies of heavy metal adsorption to sawdust were available. The goal of this paper was to acquire information on the bond length, coordination number and three-dimensional structure of copper adsorption onto natural bamboo.

The aims of this study were as follows: (i) offering an exact mechanism explanation by surface complexation models and XAFS (ii) laying the theoretical ground for the application of other adsorption materials with cellulose or lignin as the main components and providing reference for the design and synthesis of other adsorption material.

2. Materials and methods

2.1. Materials and reagents

The bamboo sawdust was the same as part 1 of this series (Zhao et al., 2012). All solutions were prepared from deionized water and chemicals were from Sinopharm Chemical Reagent Co. Ltd. Cu(NO$_3$)$_2$ stock solutions were prepared using high-purity (A.R.) reagents and adjusted to pH 2 before usage.

2.2. Sorption studies

20 g/L sawdust suspension was added into a 250 mL conical flask. Ionic strength, pH, and metal concentration of the suspension were adjusted with KNO$_3$, HNO$_3$, KOH, and Cu(NO$_3$)$_2$, respectively. Adsorption edges covered the pH range 3.5–8.5. The suspension was equilibrated for 4 h under a fully turbulent hydraulic condition at room temperature 22 ± 1 °C. The initial and final pH was measured and the supernatant was filtered through a 0.45-μm

cellulose acetate membrane. The Cu concentration in the filtrate was determined by AAS (type AA-400, Perkin-Elmer Corporation).

The above experiment was repeated with the sawdust concentration of 10 g/L and 30 g/L.

2.3. Nonelectrostatic surface complexation model

A nonelectrostatic surface complexation model (Kohler et al., 2004; Marmier & Fromage, 1999) was used to describe the metal ion adsorption data. Proton dissociation from ligands on sawdust surfaces can be described by equilibrium reaction (1) in Table 1. The concentration of proton bonding surface sites and the acidity constants can be quantified with the corresponding mass action equation which had been done in part 1 of this series (Zhao et al., 2012). The complexation of a metal ion with sawdust can be described by the following equilibrium reactions (2)–(5) in Table 1. The equilibrium constant values for the metal ion sorption reactions were calculated using the computer program FITEQL 4.0 (Herbelin & Westall, 1999). It iteratively optimizes a set of equilibrium constant by minimizing the differences between calculated and experimental data using a nonlinear least squares optimization routine. The goodness-of-fit was quantified by the overall variance (the weighted sum of squares of residuals divided by the degree of freedom, WSOS/DF).

2.4. XAFS studies

XAS data of standard samples Cu(OH)$_2$, Cu(CH$_3$COO)$_2$H$_2$O and Cu$_3$(PO$_4$)$_2$ solid powder (A.R.) and Cu(NO$_3$)$_2$ solution (pH < 1 adjusted with HNO$_3$) were acquired at the National Synchrotron Radiation Laboratory (NSRL), where the electron beam energy was 800 MeV with a maximum beam current of 200 mA. The measurements were carried out in the transmission mode with a Si (1 1 1) channel-cut monochromator.

Several samples with different initial pH and initial copper ion concentrations were used in XAFS experiments. For example, sample "CupH7.76-10mg" represented that the initial copper ion concentration was 10 mg/L and the initial pH was 7.76. After adsorption, the supernatant was filtered through a 0.45 μm cellulose acetate membrane on which the sawdust sample was transferred into self-sealed plastic bags later on. A little moisture was retained in the sawdust to ensure that its physicochemical properties did not differ too much from its aqueous solution.

XAFS data of sawdust adsorption samples were acquired at the Shanghai synchrotron radiation sources (SSRF), where the electron beam energy was 3.5 GeV. The measurements were carried out in the fluorescence mode with an Si(1 1 1) channel-cut monochromator. The detectors were low-pressure air-filled ionization chambers,

where a nickel fluorescence filter was used for scans at the Cu K-edge.

Each spectrum is the sum of three to four recordings in the range from 150 eV below to 700–1000 eV above the absorption edge. The EXAFS spectra were analyzed by NSRLXAFS 2.0 software package with phase and amplitude functions generated by FEFF (Xia, Bleam, et al., 1997; Xia, Mehadi, et al., 1997) to yield a radial structure function (RSF) and the curve fitting was performed for k^3 weight $\chi(k)$ at the wave number interval 2.2–10.5 Å^{-1}.

3. Results and discussion

3.1. The fitting by surface complexation model

Typically, the adsorption of metal ions strongly depends on pH. Not only does pH affect the condition at adsorbent surface sites, but also the hydration state of metal ions in the aqueous phase. As shown in Fig. 1, sawdust adsorption capacity for copper ions increases as pH increases. When the initial concentration of copper ion changed from 10 mg/L to 25 mg/L, the driving force for adsorption strengthened and the adsorption capacity per unit of sawdust enhanced (shown in Supplementary Material) but the removal efficiency decreased (Fig. 1). When sawdust concentration increased from 10 g/L to 30 g/L, the adsorption capacity per unit of sawdust decreased. This was because with higher sawdust concentration, the amount of copper ions contacted by sawdust reduced, resulting in weaker adsorption driving force. The increase of ionic strength suppressed copper ion adsorption, but such impact was negligible when pH was above 7.

pH dependence of metal ion adsorption can also be reflected by pH edge curves (Fig. 1). Dzombak and Morel (1990) performed a literature review and found that within the data that can be described by surface complexation models, 83% were pH boundary curves and the rest 17% were equilibrium isotherms. This suggests that the equilibrium constants of the surface complexation models cannot be applied to wider ranges of metal concentrations (Dyer, 2002). In this study, the authors also attempted to fit adsorption isotherms with surface complexation models, but the fitting was poor (not shown in the paper).

According to part 1 of this series (Zhao et al., 2012), sawdust surface was composed of high proton affinity sites (represented by "YOH"), low proton affinity sites (represented by "XOH") and permanently charged sites (represented by "ZK"). Mono-dentate and bi-dentate complexation reactions can occur at high proton affinity sites and low proton affinity sites, as shown by reactions (2)–(5) in Table 1, where >SOH represents both high proton affinity sites and low proton affinity sites. These sites can also react with some hydrated ions. The conformation of hydrated ions are often complicated (Baes & Mesmer, 1976). Among them, CuOH$^+$ is the simplest hydrated ion that can participate in adsorption most easily.

Ion exchange reaction mainly occurs at permanently charged sites where copper ions can replace potassium ions. The non-electrostatic model cannot distinguish inner complexation and outer complexation (Dyer, 2002). Although reactions (2)–(5) are in the form of inner complexation, they does not rule out the possibility of outer complexation in the reaction between metal ions and sawdust.

The amount of hydrated copper ions increased as increasing pH (Baes & Mesmer, 1976). The fitting results in Table 2 accounted for the fact that certain proportion of hydration ion CuOH$^+$ (10–30%) participates in the reaction. The goodness of fitting was better than the fitting (shown in Supplementary Material) without considering CuOH$^+$, as dictated by the lower WSOS/DF (Herbelin & Westall, 1999) ratio. The absolute value of YOCu$^+$ fitting constants were higher when YOCuOH complex was included (shown in Supplementary Material and Table 2), indicating that the
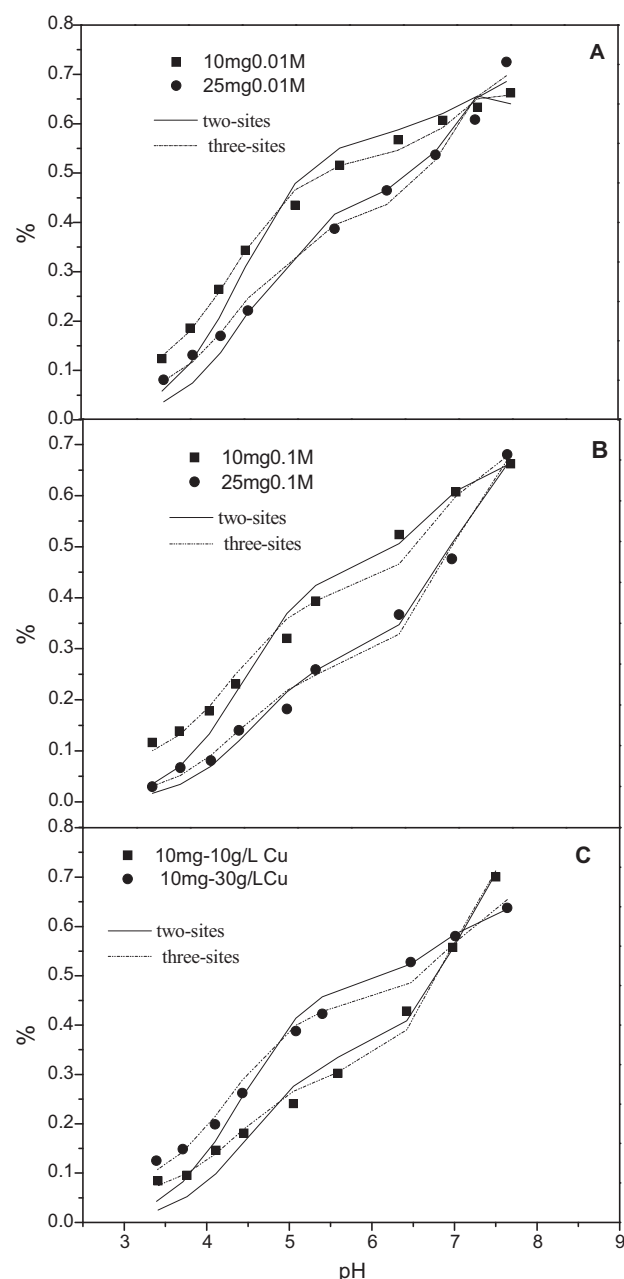

Fig. 1. Fitting curve of Cu^{2+} adsorption pH edge curves by surface complexation model (A) 0.01 M KNO$_3$, (B) 0.1 M KNO$_3$, and (C) with sawdust concentration changed.

absolute value of hydrolysis reaction constant was fairly high (Wei, 2003) and the binding strength between CuOH$^+$ and sawdust was much stronger. James argued that when hydrated hydroxyl ions were formed, the average charge was reduced, salvation energy decreased, so adsorption was abruptly enhanced (James & Healy, 1972).

In addition, the model fitting shows that CuOH$^+$ tends to bind at high proton affinity sites, considering that the fitting results including YOCuOH are better than those including XOCuOH (not shown in the table).

From Table 2, three-sites model fitted data better than two-sites model, suggested that ion exchange reaction of permanently charged sites did exist. The value of log K_{Z_2Cu} was between 4 and 6, so the binding strength was weak. As other reactions were greatly affected by the pH, its importance was highlighted at low pH. From

Table 2
Fitting parameter of surface complexation models of copper adsorption pH edge curve considering other complex forms.

Sample		$\log K_{XOCu^+}$	$\log K_{20\% YOCuOH+80\% YOCu+}$	$\log K_{Z_2Cu}$	WSOS/DF	Note
10 mg 0.01 M	Two-sites	−1.55	−5.79		5.83E−05	
	Three-sites	−1.41	−5.75	5.69	7.24E−06	Figs. 1A and 2A
25 mg 0.01 M	Two-sites	−1.78	−5.64		2.35E−04	
	Three-sites	−1.62	−5.64	5.40	1.15E−04	Figs. 1A and 2B
10 mg 0.1 M	Two-sites	−1.70	−5.07 (10% YOCuOH)		6.17E−05	
	Three-sites	−1.56	−5.06 (10% YOCuOH)	5.48	2.52E−05	Figs. 1B and 2C
25 mg 0.1 M	Two-sites	−2.03	−5.80		1.02E−04	
	Three-sites	−1.82	−5.83	4.68	1.04E−04	Figs. 1B and 2D
10 mg 0.1 M 10 g/L	*Two-sites*	*−1.94*	*−6.30 (30% YOCuOH)*		*7.14E−05*	
	Three-sites	*−1.80*	*−6.34 (30% YOCuOH)*	*5.39*	*3.90E−05*	
	Two-sites	−1.61	−6.14 (30% YOCuOH)		3.80E−05	
	Three-sites	−1.46	−6.14 (30% YOCuOH)	5.92	1.64E−05	Figs. 1C and 2E
10 mg 0.1 M 30 g/L	*Two-sites*	*−1.68*	*−5.64*		*1.39E−04*	
	Three-sites	*−1.55*	*−5.68*	*5.56*	*8.57E−05*	
	Two-sites	−1.83	−6.10		5.08E−05	
	Three-sites	−1.67	−6.08	5.11	1.53E−06	Figs. 1C and 2F

Annotation: for Sample "10mg0. 1M-30g/L", "10mg" represents the initial copper ion concentration, "0.1M" represents potassium nitrate concentrations 30g/L" represents sawdust concentration. Other with, hereinafter the same.

Fig. 1, three-sites model can significantly improve the fitting of data points at low pH. From Fig. 2, about 5–10% copper binding can be attributed to the ion exchange reaction with ZK. It shows that copper ions mainly complex onto lignin in sawdust rather than cellulose (Gode, Atalay, & Pehlivan, 2008).

Sample "10mg0.1M-10g/L" and "10mg0.1M-30g/L" were somewhat special as their sawdust concentrations were different from those used in acid–base titration experiments in part 1 of this series (Zhao et al., 2012). The italicized data in Table 2 was the fitting data inheriting completely acid–base titration fitting parameters in Table 2 of part 1 of this series (Zhao et al., 2012). Note that experimental errors did exist due to the difference in sawdust site density in acid–base titration and metal adsorption. The non-italicized data in Table 2 was the fitting data of sawdust site density multiplied by correction coefficients (correction coefficient for 10 g/L samples is 0.5, for 30 g/L samples is 1.5). Experimental errors also existed because acid–base titration constants of 10 g/L or 30 g/L were different from those of 20 g/L. By comparing the two fitting methods, it was found that the latter fitted data better, which suggested that the errors in acid–base titration constant error were smaller.

Fig. 2 was obtained by the best fitting data in Table 2. As shown by Fig. 2, XOCu$^+$ plays a leading role when pH < 6. When pH > 6, the proportion of YOCu$^+$ gradually increased. Compared to adsorption constants in Table 2, the binding ability of high proton affinity sites was higher than low proton affinity sites. However, copper ion adsorption was in fact a competition adsorption with hydrogen ions (Shukla et al., 2002). Thus, under low pH conditions, the binding of copper ions to high proton affinity sites was not dominant.

By comparing A–D sub-figures, it was found that the proportion of XOCu$^+$ decreased as the increase of initial copper ion concentration and ionic strength. As the competition ability of copper ions and hydrogen ion enhances, the binding proportion of high protons affinity sites increased accordingly. As for F sub-figure, with increasing sawdust concentration, the number of adsorption sites increased. For unit site, the competition ability of copper ions dropped, resulting in a lower binding proportion of high protons affinity sites. With the same reason, E sub-figure and F sub-figure showed an opposite trend.

The effect of ionic strength indicated that a certain proportion of the binding of copper ions to low proton affinity sites could be attributed to outer complexation which was vulnerable to the change of KNO$_3$ concentration (Koretsky, 2000). This gave a good explanation to Fig. 1, at high pH conditions, the effect of ionic strength diminishes due to the fact that the binding of copper ions to high protons affinity sites was mainly inner complexation. When fitting adsorption data, it was found that replacing 20% YOCuOH with 20% bidentate binding YO$_2$Cu at the high proton affinity sites can still yield good fitting results (not shown in the paper). The possibility of forming bidentate complex was small as explained below: when pH was higher than 6, hydrated copper ions gradually formed. Complex YOCuOH was more likely to participate in the reaction. In the research of metal ion adsorption onto mineral surface, Davis and Kent (1978) found that particle surface might induce hydrolysis, resulting in a lower pH required for the hydrolysis of metal ions on surface than that in an aqueous solution (Davis & Kent, 1978). In addition, due to the steric effect, organic matter can hardly forms bi-dentate complex with metal ions (Bartschat, Cabaniss, & Morel, 1992; Bose & Reckhow, 1997).

3.2. The analysis of binding property

Figs. 3 and 4 were XANES and its first-order derivative figure of Cu adsorption samples and standard samples, respectively. From Fig. 3, XANES spectra for Cu adsorption samples were similar among each other, but greatly differ from standard samples. Multiple scattering of sample Cu(OH)$_2$ can occur in high E space (Scheidegger et al., 1996), so its difference from Cu adsorption samples was expected. The difference with Cu(NO$_3$)$_2$ indicated that the binding of copper ions onto sawdust was substantially different from the binding occurring in aqueous phase. Generally, low protons affinity sites in sawdust consisted mainly of carboxylic acid groups, but the difference with Cu(CH$_3$COO)$_2$ indicated that many other types of sites also contributed to the binding of copper ions. Although Cu$_3$(PO$_4$)$_2$ and adsorption samples was closest, the binding of copper ions onto sawdust may merely share a common structure feature with Cu$_3$(PO$_4$)$_2$ as sawdust contained trace amount of phosphorus (Zhao et al., 2012).

From XANES spectra of standard samples, low energy shoulder peak of K absorption edge was observed, which was due to 1s → 4p electronic transition of copper ions (Alcacio et al., 2001; Xia, Bleam, et al., 1997; Xia, Mehadi, et al., 1997). Cu(CH$_3$COO)$_2$ and Cu(OH)$_2$ had the most obvious shoulder peak which were less obvious for Cu$_3$(PO$_4$)$_2$ and Cu(NO$_3$)$_2$. But from Fig. 4, the split of α and β peaks can be observed in standard samples and "CupH7.76" series of samples. The positions of α and β peaks were fairly close in "CupH7.76" series of samples (except for "CupH7.76-10mg" which was affected more by poly-nuclear hydrolysis complexes; this will be discussed next), but very different from standard samples even Cu$_3$(PO4)$_2$.
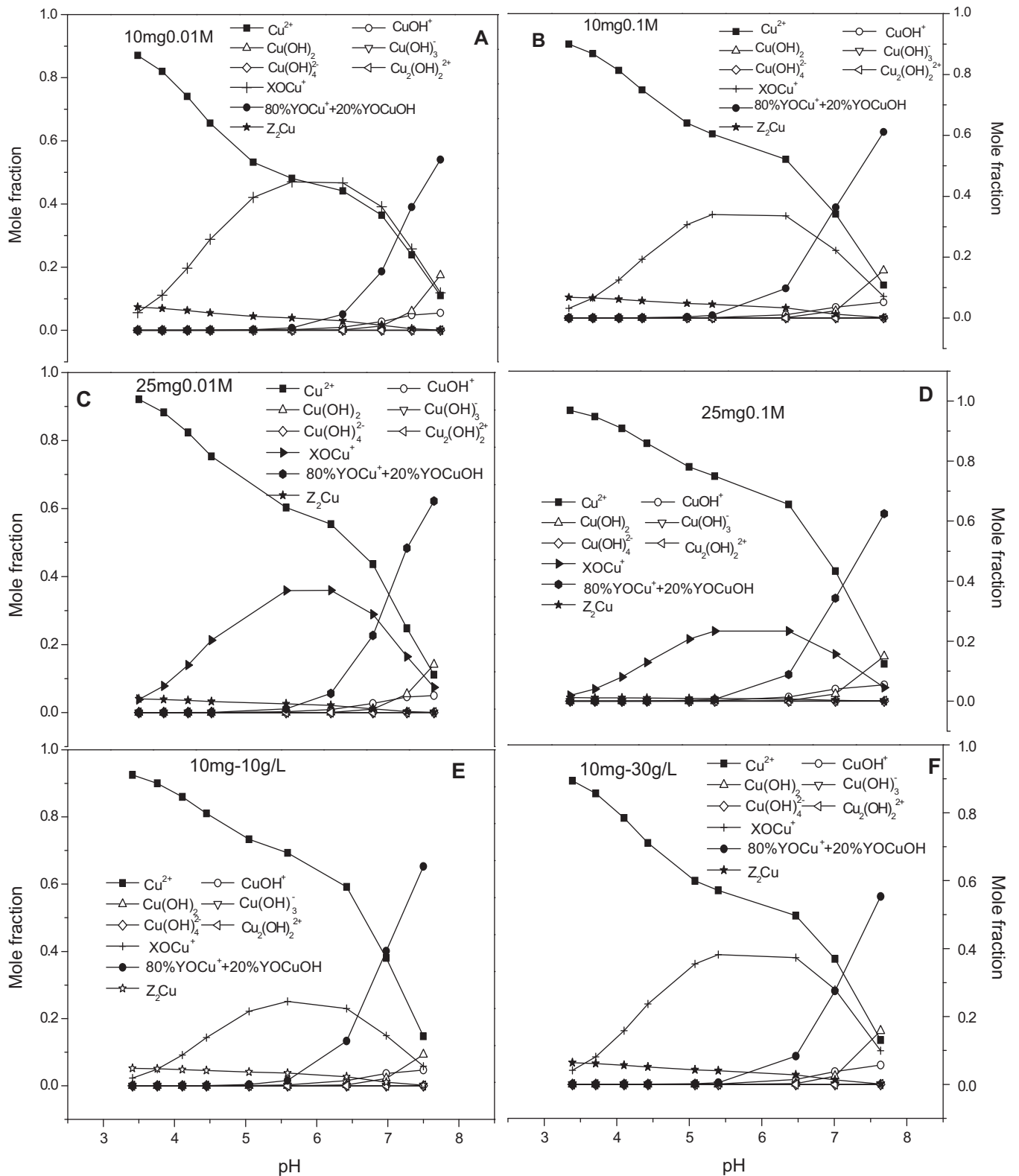
Fig. 2. Speciation diagram of Cu^{2+} adsorption.

α peak represents $1s \rightarrow 4p$ electronic transition, β peak represented the main absorption transition ($1s \rightarrow$ continuum). The split of the peak showed that weak shoulder peak structure of K adsorption edge indeed existed, and revealed the quadrilateral distortion of copper octahedron structure (Alcacio et al., 2001; Xia,

Bleam, et al., 1997; Xia, Mehadi, et al., 1997). For $Cu(CH_3COO)_2$ and $Cu(OH)_2$, the average axial distance of Cu surrounding atoms are 2.42 and 2.63 Å (Dupont et al., 2002), α and β peak energy differences were 6 eV and 7 eV, respectively. According to the energy difference between α and β peak in Fig. 4, for samples

Fig. 3. XANES figure of copper adsorption samples and standard samples.

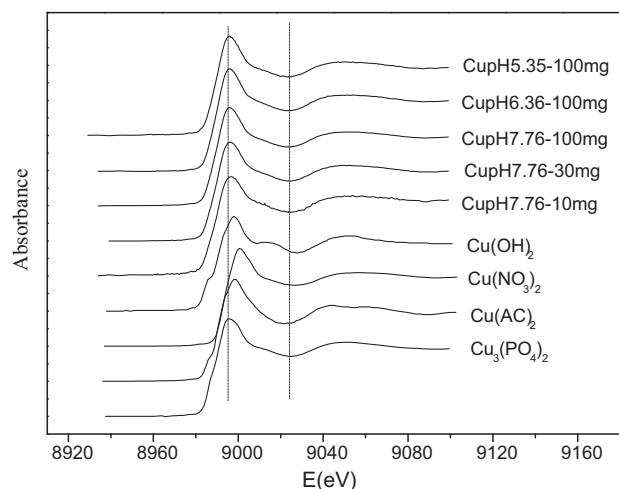**Fig. 4.** First-order derivative figures of XANES of copper adsorption samples and standard samples.

"CupH7.76-10mg", "CupH7.76-30mg", "CupH7.76-100mg" the average axial distance between Cu atoms and around axial atoms can be roughly estimated to be 2.27, 2.02 and 2.10 Å, respectively. The α peak intensity for Sample "CupH5.35-100mg" and "CupH6.36-100mg" was very low, indicating that copper ions did not form octahedron structure.

Compared to standard samples, the α peak intensity of adsorption samples decreased significantly. Typically, α peak intensity is affected by the property of ligands in equatorial direction (Kau et al., 1987). The source of α electron transition had been boiled down to a shakedown effect, where the final electronic state was lower in energy than the direct $1s \rightarrow 4p$ transition. The path to the final state involved a $1s \rightarrow 4p_z$ excitation combined with a ligand-to-metal charge transfer (Blair & Goddard, 1980). The energy of the shakedown should decrease as the ligand ionization energy decreases (Kau et al., 1987). In aqueous solution, the trend of ligand ionization was more obvious than surface sites of sawdust including hydroxyl of CuOH$^+$ which were a little more obvious than surface sites of sawdust. Take Cu(NO$_3$)$_2$ as an example, copper ions complex water molecules in a equatorial direction which generated an obvious α peak. CuOH$^+$ had a hydroxyl and participated in reaction gradually with increasing pH. So "CupH7.76" series of samples had a weak α peak compared with other adsorption sample. Another explanation was that since sawdust particles were far bigger than the water molecule in size, it produced a spatial steric effect, making it impossible to complex copper ion at the same angle in the equatorial direction. Such steric hindrance would affect the ability of ligand-to-metal charge transfer (Dupont et al., 2002). Compared "CupH7.76" series of samples with other adsorption sample, CuOH$^+$ participated in reaction, which caused spatial steric effect decrease a bit. Steric effect resulting from sawdust can also cause the octagonal distortion. α peak intensity was also affected by axial distortion (Garcia et al., 1989).

Fig. 5 was the weighted K space EXAFS spectrum of k^3 ranging from 2.3 to 10.5 Å. The peak shape of Cu(OH)$_2$ in high K space was more complex, suggesting the occurrence of multiple scattering (Scheidegger et al., 1996). Cu(CH$_3$COO)$_2$ in low K space had a dual peak, while other adsorption samples compared closely to standard samples. This indicated that carboxylic acid groups were not responsible for the binding of copper ions onto low proton affinity sites, or at least, the contribution from carboxylic acid groups was relatively small. This was somewhat different from many literatures (Dupont et al., 2002; Guo et al., 2008). Radial structure function (R space) was obtained from K space data by Fourier transformation. According to Figs. 3 and 5, Cu$_3$(PO$_4$)$_2$ and sawdust adsorption sarmples share the closest structure features. This paper
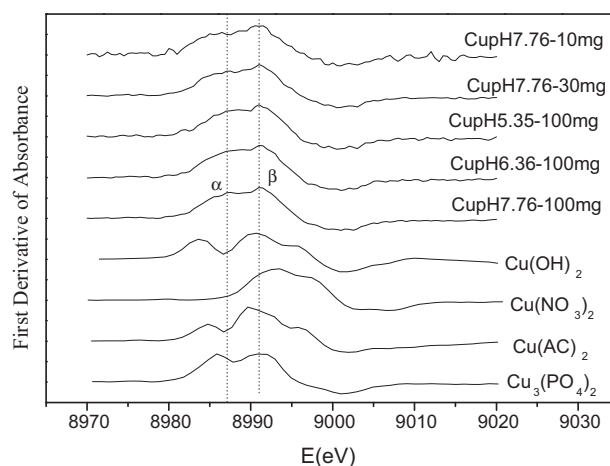
adopted phase and amplitude functions of Cu$_3$(PO$_4$)$_2$. Coordination number (N), bond length (r), Debye–Wall factor (σ_t), relative error (RE), were obtained by nonlinear least squares fitting of the first shell data of R space (Table 3).

According to the fitting without sub-shell (Table 3), the coordination number of adsorption samples was about 4, indicating that tetrahedron structure was formed. Assuming copper ions form octahedron structure with sawdust in aqueous phase, the copper ions in the equatorial direction form the first sub-shell and those in the axial direction form the second sub-shell. Due to the fact that axial and equatorial atoms were not closely related (Joyner, 1980), axial atoms may be overlooked during the fitting without considering sub-shell fitting, resulting in an underestimation of coordination number. From fitting results, the incorporation of sub-shell had negligible influence on "CupH6.36-100mg" and "CupH5.35-100mg", suggesting that low pH samples mainly formed tetrahedron configuration. In addition, the proportion of axial binding was very small and the bond length of second sub-shell only changed slightly, which corresponded well with XANES fitting results.

For pH7.76 series of samples, the consideration of sub-shell led to better fitting. However, the sum of coordination number of two sub-shells did not reach 6, indicating that the binding of copper ions and sawdust had transition configuration from tetrahedron to octahedron. Overall, as pH increased (for the series samples of pH 7.76, low copper ion concentration corresponded to high
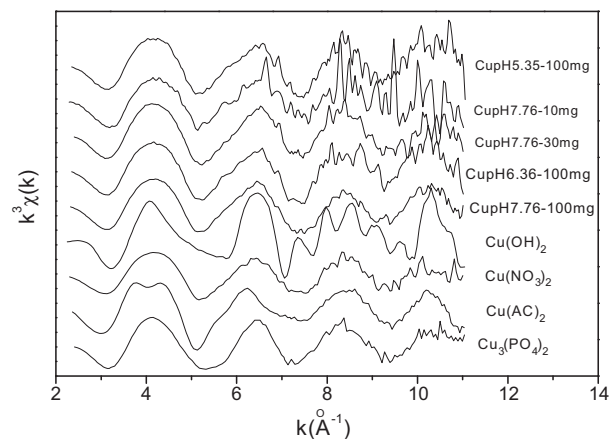

Fig. 5. K space diagram of EXAFS spectra of copper adsorption samples and standard samples.

Table 3
Fitting parameter values of first shell of copper adsorption samples.

Sample	The first shell	The first shell	
		The first sub-shell	The second sub-shell
CupH7.76-10mg			
N	4.09	3.50	1.54
σ_t	0.0885	0.0885	0.0885
r (Å)	1.92	1.92	2.52
RE	0.0366	0.0300	
CupH7.76-30mg			
N	4.54	4.66	0.939
σ_t	0.0800	0.0800	0.0800
r (Å)	1.95	1.96	2.34
RE	0.0213	0.0113	
CupH7.76-100 mg			
N	4.14	4.27	0.806
σ_t	0.0800	0.0800	0.0800
r (Å)	1.96	1.96	2.33
RE	0.0320	0.0280	
CupH6.36-100 mg			
N	4.32	3.82	0.499
σ_t	0.0677	0.0746	0.0746
r (Å)	1.97	1.97	1.96
RE	0.0350	0.0350	
CupH5.35-100 mg			
N	3.69	3.69	0.00500
σ_t	0.0598	0.0598	0.0598
r (Å)	1.97	1.97	1.97
RE	0.0310	0.0310	

pH after reaction), the sum of coordination numbers of two sub-shells also increased, suggesting that hydrated CuOH$^+$ complex may participate in the reaction. Since CuOH$^+$ bore a hydroxyl, Cu coordination number will increase when it bound with sawdust (Dzombak & Morel, 1990). This was consistent with fitting results of surface complexation models. On the other hand, the coordination numbers of sample "CupH7.76-10mg" and "CupH7.76-30mg" did not change substantially as some poly-nuclear hydrolysis complexes may also participate in reaction. The reaction mechanism was relatively complicated. In addition, with the rise of pH, equatorial bond length gradually shortened because the structures of complexes formed at low pH were closer to tetrahedron and the tetrahedral bond length was longer than the octahedron bond length in the equatorial direction. For sample "CupH7.76-10mg" and "CupH7.76-30mg", axial bond lengths reached 2.52 and 2.34 Å, which were much higher than the estimated results from XANES. However, XANES and EXFAS spectrum gave a similar explanation for copper adsorption.

4. Conclusion

The adsorption of copper ions onto natural bamboo sawdust (a kind of carbohydrate natural polymer) strongly depends on pH, copper loadings and ion strength. The results of copper pH edge curve fitted by NEM surface complexation models showed that: three-sites model incorporating permanent charge ion exchange reaction fitted better than two-sites model. Fitting result including the hydration ion reaction was better. XAFS research showed that: XANES and EXFAS spectrum gave a similar explanation for copper adsorption in spite of experimental and fitting errors. Copper ion mainly formed inner complex with sawdust, and obvious evidence about carboxylic acid groups in the combination with copper ion was not found. Space configuration of copper ions changed from tetrahedron to octahedron as the rise of pH, and the rise of coordination number indicated that hydration copper ions participated adsorption reaction. This basically ruled out the possibility of bi-dentate complexation reactions.

Appendix A. Supplementary data

Supplementary data associated with this article can be found, in the online version, at doi:10.1016/j.carbpol.2012.02.069.

References

Ahmed, S. A. (2011). Batch and fixed-bed column techniques for removal of Cu(II) and Fe(III) using carbohydrate natural polymer modified complexing agents. *Carbohydrate Polymers*, *83*, 1470–1478.

Alcacio, T. E., Hesterberg, D., & Chou, J. W. (2001). Molecular scale characteristics of Cu(II) bonding in goethite–humate complexes. *Geochimica et Cosmochimica Acta*, *65*, 1355–1366.

Baes, C. F., & Mesmer, J. R. E. (1976). *The hydrolysis of cations*. New York: John Wiley.

Bartschat, B. M., Cabaniss, S. E., & Morel, F. M. M. (1992). Oligoelectrolyte model for cation binding by humic substances. *Environmental Science and Technology*, *26*, 284–294.

Blair, R. A., & Goddard, W. A. (1980). Abinitio studies of the X-ray absorption edge in copper complexes. I. Atomic Cu^{2+} and Cu(II)Cl$_2$. *Physical Review B*, *22*, 2767–2776.

Bose, P., & Reckhow, D. A. (1997). Modeling pH and ionic strength effects on proton and calcium complexation of fulvic acid: A tool for drinking water-NOM studies. *Environmental Science and Technology*, *31*, 765–770.

Davis, J. A., & Kent, D. B. (1978). Surface ionization and complexation at the oxide/water interface. II. Surface properties of amorphous iron oxyhydroxide and adsorption of metal ions. *Journal of Colloid and Interface Science*, *b67*, 90–107.

Dupont, L., Guillon, E., & Bouanda, J. (2002). EXAFS and XANES studies of retention of copper and lead by a lignocellulosic biomaterial. *Environmental Science and Technology*, *36*, 5062–5066.

Dyer, J.A. (2002). Advanced approaches for modeling trace metal sorption in aqueous systems. Ph.D. Dissertation, The University of Delaware, Newark.

Dzombak, D. A., & Morel, F. M. M. (1990). *Surface complexation modeling. Hydrous ferric oxide*. New York: John Wiley & Sons.

Garcia, J., Benfatto, M., Natoli, C. R., Bianconi, A., Fontaine, A., & Tolentino, H. (1989). The quantitative Jahn–Teller distortion of the Cu^{2+} site in aqueous solution by XANES spectroscopy. *Chemical Physics*, *132*, 295–307.

Gode, F., Atalay, E. D., & Pehlivan, E. (2008). Removal of Cr(VI) from aqueous solutions using modified red pine sawdust. *Journal of Hazardous Materials*, *152*, 1201–1207.

Guo, X. Y., Zhang, S., & Shan, X. Q. (2008). Adsorption of metal ions on lignin. *Journal of Hazardous Materials*, *151*, 134–142.

Herbelin, A., & Westall, J. (1999). *FITEQL: A computer Program for determination of chemical equilibrium constants from experimental data. Version 4.0*. Corvallis, OR: Department of Chemistry, Oregon State University.

James, R. O., & Healy, T. W. (1972). Adsorption of hydrolyzable metal ions at the oxide–water interface. III. A thermodynamic model of adsorption. *Journal of Colloid and Interface Science*, *40*, 65–81.

Joyner, R. W. (1980). An extended X-Ray absorption fine structure (exafs) study of copper(II) sulphate pentahydrate. *Chemical Physics Letters*, *72*, 162–164.

Kau, L. S., Spira-Solomon, D. J., Penner-Hahn, J. E., Hodgson, K. O., & Solomon, E. I. (1987). X-ray absorption edge determination of the oxidation state and coordination number of copper. Application to the type 3 site in Rhus vernicifera laccase and its reaction with oxygen. *Journal of the American Chemical Society*, *109*, 6433–6442.

Kohler, M., Curtis, G. P., David, E., Meece, D. E., & Davis, J. A. (2004). Methods for estimating adsorbed uranium(VI) and distribution coefficients of contaminated sediments. *Environmental Science and Technology*, *38*, 240–247.

Koretsky, C. (2000). The significance of surface complexation reactions in hydrologic systems: A geochemist's perspective. *Journal of Hydrology*, *230*, 127–171.

Lee, B. G. (2001). *Heavy metal ion sorption of unmodified and modified lignocellulosic fibers*. Madison: University of Wisconsin-Madison.

Marmier, N., & Fromage, F. (1999). Comparing electrostatic and nonelectrostatic surface complexation modeling of the sorption of lanthanum on hematite. *Journal of Colloid and Interface Science*, *212*, 252–263.

Naiya, T. K., Bhattacharya, A. K., & Das, S. K. (2008). Adsorption of Pb(II) by sawdust and neem bark from aqueous solutions. *Environmental Progress*, *27*, 313–328.

Ravat, C., Dumonceau, J., & Monteil-Rivera, F. (2000). Acid/base and Cu(II) binding properties of natural organic matter extracted from wheat bran, modeling by the surface complexation model. *Water Research*, *34*, 1327–1339.

Reddad, Z., Cerente, C., Andres, Y., & Clolrec, P. L. (2002). Modeling of single and competitive metal adsorption onto a natural polysaccharide. *Environmental Science and Technology*, *36*, 2242–2248.

Scheidegger, A. M., Lamble, G. M., & Sparks, D. L. (1996). Investigation of Ni sorption on pyrophyllite: An XAFS study. *Environmental Science and Technology*, *30*, 548–554.

Shukla, A., Zhang, Y. H., Dubey, P., Margrave, J. L., & Shukla, S. S. (2002). The role of sawdust in the removal of unwanted materials from water. *Journal of Hazardous Materials*, *B95*, 137–152.

Steinike, U., Lutz, W., Wark, M., & Jancke, K. (1994). Detection of side-products on heavy metal cations loaded zeolites by XRD measurements. *Crystal Research and Technology*, *29*, 149–155.

Wei, J. F. (2003). Study on interface reactions of important sedimentary minerals and corresponding environmental implication. Ph.D. Dissertation, Guangzhou: Guangzhou Institute of Geochemistry, Chinese Academy of Sciences.

Xia, K., Bleam, W., & Helmke, P. A. (1997). Studies of the nature of Cu^{2+} and Pb^{2+} binding sites in soil humic substances using X-ray absorption spectroscopy. *Geochimica et Cosmochimica Acta*, *61*, 2211–2221.

Xia, K., Mehadi, A., Taylor, R. W., & Bleam, W. F. (1997). X-ray absorption and electron paramagnetic resonance studies of Cu(II) sorbed to silica: Surface-induced precipitation at low surface coverages. *Journal of Colloid and Interface Science*, *185*, 252–257.

Xu, Y., Axe, L., Yee, N., & Dyer, J. A. (2006). Bidentate complexation modeling of heavy metal adsorption and competition on goethite. *Environmental Science and Technology*, *40*, 2213–2218.

Yasemin, B., & Zek, T. (2007). Removal of heavy metals from aqueous solution by sawdust adsorption. *Journal of Environmental Sciences*, *19*, 160–166.

Yu, L. J., Shukla, S. S., & Dorris, K. L. (2003). Adsorption of chromium from aqueous solutions by maple sawdust. *Journal of Hazardous Materials*, *B100*, 53–63.

Zhao, X. T., Zeng, T., Hu, Z. J., Gao, H. W., & Zou, C. Y. (2012). Modeling and mechanism of the adsorption of proton onto natural bamboo sawdust. *Carbohydrate Polymers*, *87*, 1199–1205.